HHS Public Access

Author manuscript

Q Magn Reson Biol Med. Author manuscript; available in PMC 2015 November 05.

Published in final edited form as:

Q Magn Reson Biol Med. 1994 ; 1(2): 89–106.

Magnetic Resonance Imaging and Spectroscopy: Application to Experimental Neuro-Oncology

Brian D. Ross[1,0], **Thomas L. Chenevert**[1], **Boklye Kim**[1], and **Oded Ben-Yoseph**[1]

[1]Department of Radiology, University of Michigan, School of Medicine, Kresge III Research Building, Room R3315, Box 0553, Ann Arbor, MI 48109-0553 USA

[2]Department of Biological Chemistry, University of Michigan, School of Medicine, Kresge III Research Building, Room R3315, Box 0553, Ann Arbor, MI 48109-0553 USA

Summary

The development and use of animal brain tumor models over the past 25 years has helped to advance our understanding of both tumor biology and the effectiveness of new therapeutic approaches. The application of MRI and MRS as noninvasive tools for *in vivo* studies of intracerebral tumor models provides unique possibilities for furthering our knowledge of brain cancer. This article provides a brief background of traditional techniques used to evaluate growth and treatment efficacy in rodent brain tumor models and overviews the use of MR for quantitating intracerebral tumor growth kinetics and therapeutic response of experimental brain tumors from work conducted in this laboratory. The application of MRI and MRS in rodent brain tumor models for evaluation of novel therapeutic approaches, including gene transfer technology, is discussed. Finally, initial results with diffusion MRI for monitoring the treatment of brain tumors is introduced.

Keywords

9L gliosarcoma; magnetic resonance imaging (MRI); magnetic resonance spectroscopy (MRS); glioma; tumor growth kinetics; tumor cell kill

Introduction

Gliomas constitute a major therapeutic problem because of their frequency of occurrence and extremely poor prognosis. Despite the use of multimodality therapy, malignant gliomas remain uniformly fatal (1). Furthermore, quantitation of the response of malignancies within the central nervous system is more difficult than in systemic cancers (2–5). Improvement in patient function is multifactorial and changes in neurological deficits may be unrelated to changes in tumor size. The use of computed tomographic (CT) and MRI scans in the clinical setting do not permit the quantitation of the tumor volume. Typically, the area of contrast enhancement is used to estimate the area of the tumor since the capillaries of malignant

[0]Author to whom correspondence should be addressed, University of Michigan, Department of Radiology, Kresge III Research Building, Room R3315, Box 0553, Ann Arbor, MI 48109-0553 USA.

Partly presented at “NMR inside biology: from models to “in vivo” Altavilla Milicia (Italy) 1994

tumors may become fenestrated and allow the contrast agent to penetrate into the peritumoral region.

Because the blood brain barrier (BBB) can be altered by administration of certain chemotherapeutic agents (5) or corticosteroids, measurement of tumor size by contrast enhancement represents an indirect estimate of tumor size. Due to the difficulty in measuring the size of intracranial, tumors, brain tumor therapeutic trials usually report median survival time and median time to progression as a quantitative measure of response. This measurement of response is used even though these parameters may not correlate with therapeutic efficacy in an individual patient. Therefore, any method which would allow for accurate quantitation of the therapeutic response in individual patients would offer tremendous advantages over current approaches. In this regard, the potential of MRS for monitoring therapy of brain tumor patients has not been fully explored to determine if specific changes in tumor metabolite levels can be correlated with therapeutic effectiveness. Human brain tumors are diverse in response to treatment and with the added complexity of obtaining accurate human tumor volume measurements, the use of a reproducible animal model for the initial evaluation of MRS is warranted. Indeed, rodent brain tumor models have played an important and vital role in the *in vivo* evaluation of novel therapeutic approaches (6).

The therapeutic response of orthotopic brain tumors has traditionally been quantitated using animal survival, tumor weights following excision or colony forming assays of cells cultured from the *in situ* tumor as biological end points (7–17).

These methods have proved valuable for *in vivo* testing of new therapeutic approaches but suffer several disadvantages: 1) large numbers of animals are typically required to evaluate the efficacy of a therapeutic approach since animal-to-animal tumor growth rate can vary significantly; 2) the therapeutic response of individual animals to a single agent can vary significantly; 3) these methods are not suitable for use in the clinical setting. A method such as MRI which would allow the intracranial tumor volume to be determined noninvasively and thus repeatedly monitored over the life span of individual animals would be beneficial for evaluating new therapeutic approaches.

In this paper, the application of M RI as a non-invasive tool to serially monitor the growth and therapeutic response of the intracranial rat 9L brain tumor model (7, 10) is presented. We report that MRI can be used to accurately quantitate the intracranial tumor doubling time (T_d) from serial MR images. Because MRI revealed that untreated 9L tumors grew exponentially over the entire life span of the animal, treated animals could serve as their own control's if the T_d was determined from several MRI scans before therapeutic intervention.

Examples of how tumor cell kill can be determined from MRI tumor volume growth delay measurements following several different therapeutic interventions is presented. Initial results are also presented which correlate tumor cell kill with changes in metabolite levels following treatment using MRS.

This type of correlation provides insights into specific metabolic change(s) which are indicative of therapeutic efficacy. Finally, initial results exploring the use of diffusion MRI for monitoring therapeutic effectiveness are presented. These studies are needed to more clearly define the specific metabolic parameters which correlate with therapeutic efficacy (or resistance to therapy) before the full potential of MRS can be utilized in the clinical setting.

Materials and Methods

Magnetic Resonance Imaging

All *in vivo* MR experiments were performed on a Spectroscopy Imaging Systems Corporation (SISCO) system equipped with a 7.0 Tesla, 18.3 cm horizontal bore magnet (300 MHz proton frequency). For MRI examination, rats were anesthetized with a ketamine/xylazine (87 mg/kg/13 mg/kg, i.p.) mixture and maintained at 37°C inside the magnet using a heated circulating water blanket. MRI of rat brains was initiated between 8 and 10 days following cell implantation and repeated every other day. The rat head was positioned inside a 4 cm diameter birdcage rf coil which was designed and constructed with ear bars to secure the position of the head during the acquisition. For each MRI session, a single slice gradient-recalled-echo image was acquired with 1 mm “saturation crosshairs” imprinted on the axial and coronal images to facilitate rapid and reproducible positioning of the animal. Multislice coronal images were acquired using a standard spin echo sequence. T_2-weighted images through the rat brain were produced using the following parameters: TR/TE = 3500/60, FOV= 30 × 30 mm using a 128 × 128 matrix, slice thickness = 0.5 mm and slice separation = 0.8 mm. Twenty five slices were acquired followed by acquisition of a second set of 25 slices with a slice offset of 0.4 mm providing a contiguous image data set of the rat brain.

Calibration of MRI Volume Measurements using Phantoms

Calibration of MRI volume measurements was achieved by measuring the volume of four sphere phantoms using the same MRI acquisition protocol used for scanning rats. The phantoms consisted of spherical glass bulbs and the “actual volumes” of the phantoms which were calibrated using a Hamilton Syringe were 22.5, 31.2, 113.5 and 297.7 mm^3. Phantom volumes obtained from MRI data sets were compared with the actual volume of each phantom to determine the accuracy of the MRI method.

Quantitation of Intracranial Tumor Volumes

For volume measurements at each time point, the area (volume) of tumor visualized in each slice was manually outlined using a region-of-interest (ROI) program provided with the SISCO MR software. The outlined tumor area in each cross-sectional image was multiplied by the slice separation (0.4 mm) to calculate the tumor volume in each slice. The tumor volumes of individual slices were summed to yield the total volume of the tumor. Tumors with a minimal volume of 8–10 mm^3 were used for the initial volumetric time point.

Determination of Tumor Doubling Time (T_d) and Log Cell Kill

Tumor volumes measured by MRI in individual animals were plotted against hours post cell implantation to determine the growth rate of the intracranial 9L gliomas. By using the definition of exponential growth,

$$v(t)=v_0 10^{kt} \quad (1)$$

where v(t) is tumor volume at time t, v_0 is the initial tumor volume, the volumetric T_d was calculated from the expression, $T_d = \ln 2/(k)$. The tumor growth rate constant was obtained from an exponential curve fit of the volume data points using a least squares algorithm.

Log cell kill for each treated animal was determined by using the expression for post treatment tumor volume. The post treatment tumor volume, V_P, becomes:

$$v_p(t)=(1-f_k)v(t_T)10^{k'(t-t_T)}+f_k v(t_T) \quad (2)$$

where $v(t_T)$ is tumor volume at the time of treatment, f_k is fraction of cells killed by the treatment and *k* is the post treatment growth rate constant. It is assumed that $k' = k$. The first term in equation 2 describes the growing fraction following treatment while the second term describes the dead cell fraction following treatment. In this study, equation 2 was used to model the effect of increasing cell kill on the post treatment tumor growth rate.

Given the empirical growth delay, $(T_\tau - T_C)$ which is defined as the difference in time for untreated (T_C) and treated (T_t) tumors to grow to the same size (18), cell kill can be determined by:

$$log(\text{cell kill})=(T_\tau - T_C)K \quad (3)$$

The values of T_τ, T_C and T_d can all be accurately determined from the serial MR images of the intracranial tumor, thus allowing determination of the cell kill in an individual animal.

Localized ^{1}H MRS

Water-suppressed spatially localized ^{1}H spectra were acquired using a previously described method (19). In brief, spatial localization utilized a hybrid approach by combining two-dimensional ISIS (image selected *in vivo* spectroscopy) (20) and spectroscopic imaging (SI) (21) to define contiguous slices along the axis of the ISIS column.

The adiabatic spin-echo pulse SSAP (solvent suppressive adiabatic pulse) (22) was incorporated into the ISIS-SI sequence.

The position of the ISIS column was determined from surface coil MR images (23). A 16 mm diameter surface coil was used for obtaining the surface coil MR images and for the ^{1}H MRS studies.

Cell Culture Conditions

9L glioma cells were grown as monolayers in 75-cm^2 sterile plastic flasks in modified Eagle's minimum essential medium with 10% fetal calf serum. Cells were cultured in an incubator at 37°C in an atmosphere containing 95% air and 5% CO_2 until confluent. Cells were harvested by trypsinization, counted and resuspended in serum-free media for intracerebral injection.

Induction of Brain Tumors

Intracerebral brain tumors were induced in anesthetized (ketamine 87 mg/kg + xylazine 13 mg/kg body weight, i.p.) male Fischer 344 rats weighing between 125 and 150 g. A small skin incision over the right hemisphere was made. A high speed drill was used to create a 1 mm diameter burr hole through the skull. Inoculation of 10^5 9L tumor cells in 5μl serum-free culture medium in the right forebrain at a depth of 3 mm was accomplished. The burr hole was filled with bone wax to minimize extra-cerebral extension of the tumor tissue. The skin was sutured and the rats were allowed to recover.

Treatment Protocols and Therapeutic Rationale

I. Single Chemotherapeutic Dosage Experiment Using BCNU—The use of 1,3-bis(2-chloroethyl)-1-nitrosourea (BCNU) has been shown to significantly increase the survival time of rats harboring intracerebral 9L tumors (10). To evaluate the use of MRI for quantitating treatment efficacy by changes in tumor growth rates and tumor cell kill, following the quantitation of tumor pre-treatment growth rates, rats were treated with a single i.p. injection of 13.3 mg/kg body weight (equivalent to LD_{10}). Rats were imaged every two days following the treatment to determine the changes in T_d and for evaluation of cell kill.

II. Multiple Chemotherapeutic Dosage Experiment Using FMdc—Ribonucleotide reductase is involved in DNA synthesis and has been a potential target for cancer chemotherapy. FluoromethyIene-2′-deoxycytidine (FMdc), a new ribonucleotide reductase inhibitor, has recently been reported to be active against human breast tumor xenografts (24). In order to investigate this compound against brain tumors, rats with intracranial 9L tumors were imaged 3–4 times beginning 9–10 days post cell implantation to determine the individual tumor T_d's. Following determination of tumor pre-treatment growth rates, rats were treated with daily i.p. injections of FMdc 15 mg/kg body weight. Rats were imaged every two days during the treatment protocol and several rats underwent localized ^{1}H MRS examination to determine if changes in ^{1}H metabolites could be detected and correlated with treatment efficacy.

III. Gene Therapy—A novel approach to antitumor therapy is the transfer of the herpes simplex virus thymidine kinase (HSVtk) gene into tumor cells (25). Cells which express the viral gene will then be capable of phosphorylating anti-HSV agents, such as ganciclovir (GCV) into a toxic phosphorylated derivative. Previous studies of this gene directed therapy in experimental tumor models in rodents using retrovirally mediated transfer have been promising (26–28). Furthermore, this approach is being evaluated in a clinical brain tumor trial (29). In anticipation of the human clinical trials, we sought to investigate the cytotoxic effect of Ad.RSVtk/GCV treatment using MRI to quantitate changes in tumor growth rates and to correlate these changes with changes in ^{1}H MR spectra of these tumors. The T_d of intracerebral 9L tumors was obtained from several MRI scans prior to gene therapy. A stereotaxic injection of Ad.RSVtk was then administered at a depth determined from MRI scans of the tumor obtained on the same day. Administration of Ad.RSVtk to the 9L tumor was done at approximately 16 days post tumor implantation and treatment with GCV (15 mg/kg) was initiated 24 hours post virus injection and repeated twice daily.

IV. Oxidation Therapy—We have previously defined oxidation therapy as the use of a reactive oxygen species-generating enzyme system for tumor treatment (30). Oxygen radicals induce cytotoxicity by a variety of mechanisms including DNA damage, lipid peroxidation and protein oxidation. ^{31}P MRS is useful for assessing the *in vivo* metabolic effect of oxidation therapy because hydrogen peroxide (H_2O_2), the species generated by the enzyme system, is known to deplete cellular ATP levels by two known mechanisms: 1) Activation of poly(ADP-ribose)poIymerase following H_2O_2-induced DNA strand breaks (31). Activation of poIy(ADP-ribose)poIymerase consumes NAD^+, a process that is subsequently associated with a loss of ATP levels (32–34). 2) H_2O_2-inhibition of the glycolytic enzyme glyceraldehyde 3-phosphate dehydrogenase (35). Polyethylene-modified glucose oxidase (PEG-GO) (50 or 200 units) contained in 50 μl phosphate buffered saline (PBS) was administered by an intratu-moral injection. Tumors treated with 200 units PEG-GO received a second identical injection 3 h later. Care was taken to distribute the PEG-GO as evenly as possible throughout the tumor mass. At the conclusion of the second 200 unit PEG-GO injection. 10,000 units each of PEG-superoxide dismutase and PEG-catalase was administered i.v. in order to protect the animals from systemic toxicity clue to the potential leakage of H_2O_2 and/or the PEG-GO from the tumor site into the vascular system. Control animals were treated identically except that the PEG-GO was denatured by heating at 90°C for 15 minutes prior to injection. In order to determine the effects of this therapy on cellular energy state *in vivo*, ^{31}P MR spectra were recorded on several s.q. 9L tumors at pre- and 6 h post-intratumoral injection.

V. Lonidamine (LND)—The rapid cellular proliferation and resistance to therapy exhibited by malignant gliomas is due in part to its ability to maintain essential energy metabolite levels through abnormally high rates of glucose utilization and aerobic glycolysis. Metabolites produced by the biochemical utilization of glucose include high-energy phosphate compounds such as ATP and PCr. Since LND is believed to reduce tumor glucose utilization by inhibition of the mitochondrially-bound glycolytic enzyme hexokinase (36), ^{31}P magnetic resonance spectroscopy was used to noninvasively follow the effects of LND on both tumor pH and the high-energy phosphate metabolites in subcutaneous 9L tumors. Surface coil ^{31}P s.q. 9L tumor spectra were acquired in 5 minute intervals pre- and post-LND administration (100mg/kg, i.p., dissolved in a glycine buffer).

VI. Hyperglycemia—Hyperglycemia has been previously shown to increase tumor sensitivity to hyperthermia through a reduction in tumor blood flow (TBF) and pH (37). ^{2}H and ^{31}P MRS are a excellent tools for studying TBF and tumor pH, respectively, and hence are valuable for studying the effects of hyperglycemia on tumors. Previous studies reporting the effects of hyperglycemia on subcutaneous and intracerebral C6 gliomas has been reported (38). In brief, hyperglycemia was induced by a bolus i.p. injection of an aqueous 50% glucose solution (6g/kg). ^{31}P MR spectroscopy was used to investigate the effects of hyperglycemia on C6 glioma pH and high energy metabolites over time. Hyperglycemia-induced TBF changes in subcutaneous and intracerebral C6 gliomas were quantitated using ^{2}H MRS as previously described (39).

Studies of Brain Tumor Glucose Metabolism Using ^{13}C MRS

^{13}C MR spectroscopy is a noninvasive and powerful technique for studying metabolic pathways using ^{13}C-labeled precursors. Brain tumors are believed to utilize glucose differently compared to normal brain. The ability to follow the metabolism of glucose in an intracerebral glioma model offers a unique opportunity to study brain tumor energy metabolism. Furthermore, the rate of glucose utilization may prove diagnostically useful for monitoring therapeutic efficacy or grading unknown tumors. A previous study using ^{13}C MRS to follow the metabolic utilization of (1-^{13}C)glucose in an intracerebral C6 glioma is briefly reviewed (40). All ^{13}C MR spectra were acquired on a 4.7 Tesla vertical-bore Nicolet MR system. Proton-decoupled spectra were acquired using an 8mm diameter ^{13}C surface coil probe with a concentric and coplanar 19mm ^{1}H coil. Infusion of (1-^{13}C)glucose (250 mg/ml) was accomplished through the femoral vein. Rats received an initial loading dose of 0.1 ml (1-^{13}C)glucose over the first min which was followed by a constant infusion at a rate of 0.025 ml/min using an infusion pump. ^{13}C MR spectra were acquired before, during and following infusion of (1-^{13}C)glucose.

Diffusion MRI—Diffusion studies were performed on a 2T Omega CSI system (GE NMR Instruments) using a scheme that measures water diffusion properties along a column through the brain (41). Conventional T_2-weighted MR images were used to guide positioning of the right-to-left oriented column that intersected the glioma and contralateral rat brain. The acquisition technique employs orthogonal slice-selective $\pi/2$ and π pulses to define the column, frequency encoding for localization along the column, and phase-insensitive signal averaging for immunity to motion artifact that otherwise compromise *in vivo* diffusion studies. Two diffusion sensitization gradient settings were used for calculation of apparent diffusion coefficient (ADC) via ADC = ln(Ib1/Ib2)/(b2−b1), where Ib1 and Ib2 denote measured signal intensity at diffusion sensitivities b1 and b2 respectively. Nominal "b-factors" of b1=77, b2=490sec/mm^2 were applied independently along x, y, and z directions. Diffusion anisotropy effects were minimized by calculation of ADC_{mean} = [ADCx + ADCy + ADCz]/3. All gradient settings were interleaved within a single 8.5 minute scan.

Results

Phantom Study

Comparison of the known phantom volumes versus MRI-determined volumes revealed they were in close agreement to within 10%. This suggests the MRI methodology is accurate and therefore not affected by significant partial volume effects.

MRI of Intracerebral 9L Tumors

Intracranial 9L glioma volumes could be measured by MRI approximately 10 days post-implantation (42, 43). Shown in Figure 1A–1E are a representative series of T_2-weighted coronal MR images revealing the growth of an untreated intracranial glioma from 10 to 18 days post-implantation. In this figure, the series of MR images are shown from the same region of the rat brain located at approximately the largest diameter of the tumor. The glioma is clearly evident in the right hemisphere as a hyperintense region which is easily

distinguished from the normal brain parenchyma. An increasing mass effect with time due to the presence of the expanding tumor is evident (e.g. midline shift). The characteristic features of untreated 9L tumors imaged in this study were a well demarcated tumor mass with a relatively uniform hyperintense tumor signal and minimal peritumoral edema.

Shown in Figure 2 is a semi-log plot of the volume *versus* hours post intracerebral implantation of 10^5 9L tumor cells. The individual points are shown along with the line representing the least squares fit. The T_d of the 9L tumor shown in Figure 2 was determined to be 68 hr and shows the exponential growth pattern observed for all our untreated intracerebral 9L tumors. The mean tumor doubling time of intracranial 9L gliomas determined from sequential MR measurements was 66 ± 8 hr (n = 10, ±S.D.) and ranged from 50 to 81 hr. All untreated intracerebral 9L gliomas imaged in this study were found to grow exponentially over the entire lifespan of the animal with an average correlation coefficient of 0.986 ± 0.14 (n=10, mean±S.D.) (43).

Quantitation of Therapeutic Efficacy Using MRI

In order to determine the sensitivity at which the MRI volumetric measurements could detect a change in T_d (or cell kill), the untreated rats were analyzed as if they were treated in the following manner. The first four volumetric measurements of each untreated 9L tumor were used to determine the T_d for that particular tumor.

The fourth volumetric data point (the volume at the supposed time of treatment) was used with the subsequent volume measurements along with T_d (determined from pre-treatment volumetric data) to calculate the cell kill (f_k) using an iterative fitting algorithm for equation 2.

Data analysis revealed that for all untreated rats, cell kill values ranged from ±0.1 log cell kill.

Thus, evaluation of MR tumor growth data from untreated rats showed MRI was sensitive enough to detect changes in tumor growth rates if a treatment resulted in > 0.1 log kill.

Treatment Protocols

I. 8CNU—The use of MRI also allows for monitoring changes in tumor morphology following treatment. Shown in Figure 1F–1J are a series of T_2-weighted images of an intracranial 9L tumor which was treated with BCNU at day 14 (Figure 1F). Although the tumor continued to grow for several days following treatment, at day 28 post-BCNU treatment, the 9L tumor contained relatively large and disseminated hypointen-se regions and showed evidence of regression. Figure 3 shows a semi-log plot of the volume versus time post-implantation of an intracranial 9L glioma. At approximately 1–2 hr before the third volume measurement, the rat was treated with an LD_{10} dose of BCNU. The time course of post-treatment tumor volumes shows a deviation from the well-defined pre-treatment exponential growth curve. The volume of the tumor appears to increase (although the rate of growth is attenuated) for 5–6 days after treatment followed by a decrease in tumor volume during 6–14 days post treatment. After approximately 14 days post treatment, the T_d of the intracranial 9L tumor increased to the pretreatment rate. A growth delay of 356

hr ([a]15 days) was calculated from the MRI data, and when combined with the pretreatment growth rate T_d of 50 hr, a log kill of 2.1 was calculated using Equation 3. Log kills of 2.1 and 1.8 were found for the other two rats treated with BCNU. An average survival time of 38 ± 5 days (n = 3, ±S.D.) for BCNU treated rats was found compared to the average survival time of 22 ± 2 days (n=10, ±S.D.) for untreated animals yielding a 73% increased life span for BCNU treated animals.

II. FMdc—Shown in Figure 4 is a plot over time of the MRI-determined intracerebral 9L tumor volume before and during daily administration of FMdc. This data clearly reveals a progressive decline in T_d over time during FMdc treatment. Localized ^{1}H MR spectra were also acquired during the course of FMdc treatment to determine if metabolic changes which would correlate with changes in the tumor growth rate could be detected (44, 45). Shown in Figure 5 is a T_2-weighted image of a rat brain showing the position of the ISIS column within the rat head prior to acquiring the spectroscopic data. Shown in Figure 6 are a series of ^{1}H spectra obtained from a rat brain with an untreated 9L tumor (Fig. 6A) and a 9L tumor treated for 6 (Fig. 6B) and 9 (Fig. 6C) days. The ^{1}H spectra reveal a progressive increase in the lipid/lactate resonance intensity at 1.3 ppm and a decrease in the choline (3.2 ppm) and creatine (3.0 ppm) resonances during the treatment protocol.

III. Gene Therapy—In Figure 7 a dramatic retardation in the growth rate of a 9L tumor following gene therapy using Ad.RSVtk/GCV is shown (46). In this case, the 9L tumor was infected with Ad.RSVtk following acquisition of the third volumetric data point. A 24 hr time period was allowed in order for the gene product, herpes simplex virus thymidine kinase, to be expressed within the tumor cells. GCV administration was then initiated and maintained until indicated by the downward pointing arrow. Shown in Figure 8 are ^{1}H spectra of an (A) untreated 9L tumor and (B) a 9L tumor which was treated for 7 days with GCV following infection with Ad.RSVtk. This gene therapeutic approach produced an increase in the lipid/lactate resonance as clearly shown in Figure 8B.

IV. Oxidation Therapy—Figure 9 are *in vivo* ^{31}P-MR spectra of a subcutaneous 9L tumor acquired before (Fig. 9A) and 6 hr following (Fig. 9B) intratumoral injection of 50 units PEG-GO. The spectrum obtained 6 hr post-intratumoral injection of 50 units PEG-GO revealed a significant impairment of the energy state indicated by the decrease in the PCr and ATP resonances and the increased level of P_i. However, after 24 hr, the energy state almost completely recovered (not shown) and the rate of tumor growth remained unretarded. Compared to pre-treatment ATP levels (Fig 10A), 6 hr following intratumoral injection of 2×200 units of PEG-GO (Fig. 10B) resulted in the nearly complete loss of PCr and ATP and a reciprocal increase in P_i. For 2×200 units PEG-GO treated tumors, the ATP/P_i ratio decreased by 96 ± 2% (n=3) and was accompanied by a 0.72 ± 0.10 (n=3) decline in tumor pH (30). In addition, a significant ($p<.001$) growth delay of 4 days between control and treated groups (2×200 PEG-GO) was achieved (30).

V. LND—Shown in Figure 11 is a representative example of a ^{3l}P NMR spectrum of a rat 9L glioma before (Fig. 11A), and 3 hr following LND administration (Fig. 11B). This figure reveals a dramatic decline in ATP and PCr and corresponding increase in P_i levels due to

LND. Dosage of rats with drug vehicle alone (i.e. glycine buffer) showed no changes in tumor ^{31}P NMR spectra. Figure 12 displays the average dynamic changes in glioma ß-ATP/P_i and PCr/P_i metabolite ratios obtained From 3 rats studied. Ratios of ß-ATP/P_i. and PCr/P_i were decreased 65% and 50%, respectively, over the 3 hr period studied (47). The pH declined approximately 0.45 pH units during the first 30 min and slowly rcovered to within 0.15 pH units 3 hr post-LND (Fig. 13). In contrast, minimal changes pH and metabolite levels were found to occur in normal tissues including rat brain and muscle over a 3 hr period following LND administration indicating that LND had a selective effect on tumor *versus* normal tissue metabolism. It is worthwhile to note that glioma pH, ATP and PCr levels were found to fully recover within 24 hours following a single i.p. bolus of LND (data not shown).

VI. Hyperglycemia—In order to follow the effects of hyperglycemia on TBF, changes in the washout of ^2H_2O was followed before and during glucose loading using ^{2}H MRS. Shown in Figure 13 are a series of ^{2}H spectra for a subcutaneous rat C6 glioma obtained before (Fig. 14A) and 1 hr following glucose infusion (Fig. 14B). The dramatic reduction in ^{2}H washout shown in Figure 14B revealed a significant decline in TBF induced by hyperglycemia. Using the early decay washout data, TBF was quantitated using a single-compartment model as previously described (39). For the data in Figure 14A and 14B, the tumor blood flows were 12.6 and 2.4 ml/min/100 g tissue, respectively, corresponding to an 81% reduction in TBF following glucose loading. The effects of hyperglycemia on subcutaneous C6 glioma pH using ^{31}P MRS reported the reduction in TBF also correlated with a decrease in pH by 0.8 units (38).

^{13}C MRS

The use of ^{13}C MRS for monitoring the metabolism of (1-^{13}C)glucose in an experimental brain tumor model has previously been reported (40). *In vivo* ^{13}C MR spectra of an intracerebral C6 glioma before and during (1-^{13}C)glucose infusion is shown in Figure 15A and 15B, respectively. The ^{13}C-enriched metabolites can be more clearly seen in the background-subtracted spectrum shown in Figure 15C. Metabolites present included the a and β C-1 anomers of glucose at 92.9 and 96.8 ppm, respectively, C-3 labeled lactate at 20.8 ppm, C-2, C-3 and C-4 labeled glutamate/glutamine at 55.3, 27.5 and 34.2 ppm, respectively, and (1-^{13}C)glycogen at 100.5 ppm.

Diffusion MRI

Water diffusion studies were conducted on rats bearing 9L and C6 gliomas, and BCNU-treated 9L gliomas (48). The T_2-weighted image of an untreated 9L rat brain tumor illustrates localization of the column used for diffusion study (Figure 16); the corresponding ADC plot is shown in Figure 17. The ADC_{mean} values in the 9L tumor are only moderately elevated relative to contralateral brain tissue. This result is consistent with the observed histologic properties of the 9L tumor which exhibits a highly cellular tumor mass with little or no necrosis. The C6 tumor, on the other hand, typically has necrotic regions as apparent in the T_2-weighted image in, Figure 18. The reduced cellularity and increased extracellular water space imply greater water translational mobility as confirmed by the corresponding ADC plot in Figure 19. For reference, completely unrestricted pure water diffusion would

have a value of $\approx 2.5 \times 10^{-3} mm^2/sec$. The BCNU treated 9L glioma exhibits a distinct increase in ADC_{mean} (Figure 20) relative to non-treated 9L tumor tissue. This observation may be a direct result of breakdown or loosening of the tumor cellular membranes and increased interstitial space.

DISCUSSION

Over the past two decades the prognosis for patients with primary malignant tumors of the CNS has not improved appreciably (1). Due to the complexity of influences of the host on tumor growth and response to therapy, the use of animal models for evaluating new therapeutic approaches is vital. The capability-offered by MRI and MRS to noninvasively probe the volumetric and biochemical growth characteristics of rodent brain tumor models is providing new insights into this challenging and terminal disease. The use of MRI to quantitate *in vivo* therapeutic efficacy provides a more sensitive assessment of novel treatment modalities versus traditional animal survival measurements. This is because a minimum cell kill of one log unit is needed to discern a statistically significant increase in mean life span whereas the MRI approach can detect as little as 0.2 log kill (43). Furthermore, the use of MR techniques may provide insights into the biochemical or physiological basis of non-responsiveness due to such factors as tumor size, location, growth rate, vascularity, etc. The use of MRS in the clinical setting will depend upon its capability for diagnosis, prognosis or individualization of treatment. These capabilities may be advanced through the careful correlation of specific therapeutic-induced changes in MRS-observable metabolite levels with MRI-determination of tumor cell kill using rodent brain tumor models. Evaluation of new treatment strategies using rodent brain tumor models with MRI/S offers many advantages including improving characterization of dose-response relationships, drug uptake and retention studies, mechanism of action studies, correlation of MRS-observable metabolic changes with cell kill for use in clinical evaluation of treatment, etc. These advantages should provide an improved understanding of many aspects of a given experimental treatment as well as potentially decreasing the number of animals, amount of drug and the time needed for initial evaluation.

As with most scientific techniques, the application of MRI/S to study experimental brain tumors should be assessed by its ability to increase our knowledge and understanding of the disease and the effects of treatment. MRI has provided new insights into the biology and treatment response of the 9L brain tumor model. For instance, MRI determination of tumor intracranial T_d revealed tremendous inter-animal variation which helps to explain the variation in animal survival for animals injected on the same day and with the same suspension of cells. This suggests that the variation is not simply due to differences in the number of cells delivered during the cell implantation procedure. In addition MRI revealed the exponential growth exhibited by the intracranial 9L tumor model. This was previously unknown and intracerebral 9L tumor growth rates were believed to slow as the tumors expanded as indicated from measurements of tumor weights (10). The exponential growth of intracerebral 9L tumors now provides for pre-and post-treatment MRI determination of T_d (and thus cell kill) in a single animal the reby eliminating inter-animal growth rate variability in analysis of treatment effectiveness. Furthermore, as previously mentioned, MRI provides a more sensitive assessment of treatment effectiveness than traditional animal

survival measurements. This is exemplified by the MR studies evaluating FMdc. In these studies, treatment of rats with intracerebral 9L tumors with FMdc retarded the tumor T_d. However, as the calculated cell kill was only 0.2 log/day, the use of animal survival to assess this drug would have concluded it to be ineffective as the cell kill would not have significantly increased survival over untreated animals. Furthermore, when we initially evaluated FMdc, we noted a significant tumoricidal effect at 10 mg/kg using MRI with the T_d increasing by 49±10% (n=5) (44). Because no systemic toxicity was evident, we proceeded with studies at the higher dose of 15mg/kg which resulted in a larger increase in T_d (82±9%). Although a cell kill of less than 1 log is not therapeutically useful (as is the case for FMdc at a dose of 15mg/kg), the optimal drug dosage and route of administration are not yet established for this compound. Thus, pursuit of optimal drug dosage and delivery route is warranted and would nave been overlooked by traditional methods of *in vivo* brain tumor treatment assessment. Finally, MRI also provides for monitoring morphological changes in tumor tissue following treatment (Fig. 1F–1J). This capability, combined with information on changes of tumor volume over time, can help to assess potential regional variations in tumors which are responsive, or partially responsive to treatment.

Results from multinuclear MRS studies of established experimental brain tumor models have also proved useful by providing new insights into the biochemistry and metabolic response to treatment. For example, the recent dogma was that all tumors, regardless of cell type and host tissue, were selectively sensitive to hyperglycemia as indicated by a greater than 50% reduction in TBF and acidification (49). The ^{2}H and 31_P MRS studies described above demonstrated that this is not the case as the same cell line grown in two different tissue types demonstrated a site-dependence effect to hyperglycemia. It was therefore suggested that tumors are not uniquely sensitive to hyperglycemia as previously thought and that the host tissue harboring the tumor has an important role in the regulation of TBF (38).

The use of MRS during the development of novel therapeutic approaches can be very beneficial. During our initial evaluation of oxidation therapy (30) in which we sought to determine if it was a viable approach, ^{31}P MR spectra of 9L tumors treated with 50 units of PEG-GO revealed a moderate impairment of ATP levels (see Figure 9B) but did not significantly delay tumor growth. At a higher dose, a dramatic decline in both the ATP/P_i ratio and tumor pH was noted in the ^{31}P spectrum as compared to the control group at 6 hr post-treatment. The 2×200 dose of PEG-GO also produced a significant delay in tumor growth which correlated with the impairment of energy metabolism. Although the exact mechanism(s) for these metabolic changes are yet to be delineated, the use of ^{31}P MRS for following the progress of the treatment by monitoring energy metabolites is beneficial for providing information as to the progress of the treatment. This type of feedback will play a key role for future improvements, such as using an enzyme system in which H_2O_2 production could be manipulated by substrate availability and/or direct chemical inhibition. In this example, ^{31}P could be utilized for monitoring the progress of oxidation therapy dynamically (as indicated by the level of ATP depletion) in order to determine when the generation of oxygen radicals could be discontinued. As future developments will entail optimizing the oxidase system, selective pre-sensitization of the tumor tissue, and improving methods of delivery to the tumor site, the use of MRS most certainly will have a key role.

A significant decline in glioma high-energy phosphate stores and intracellular pH also occurred following LND administration (47). This unique and selective reduction of tumor energy stores and pH by LND may be exploitable for sensitizing gliomas to radiation and/or hyperthermia. ^{31}P MRS aided in determining the time course of LND-induced changes in tumor pH and ATP levels. This is important information since it was shown in Figure 10 that the pH tended to recover over time post-LND administration. By using ^{31}P MRS to obtain a prior knowledge of when the maximal reduction of pH has occurred, the timing of the treatment can be coordinated to yield maximum sensitization. Further work is needed to establish if the metabolic changes are dose dependent and to determine whether the effects of LND on subcutaneous gliomas are reproducible on intracerebral gliomas. The changes in tumor metabolite levels observed using ^{31}P MRS were in fact consistent with a mechanism involving inhibition of the glycolytic enzyme, hexokinase (36).

The use of MRI/S for testing novel gene therapy approaches on experimental brain tumor systems provides many advantages over traditional assays. For studies in which the viral vector is stereotaxically injected into the tumor, the exact coordinates can be determined from MRI scans (46). Furthermore, the effectiveness of the approach can be evaluated by determining the change in T_d (or cell kill) from MR images of the intracerebral tumor. Many important issues remain: 1) What is the optimal time period over which the GCV should be administered? 2) Should the tumor be redosed with the viral vector at a later time period? 3) Does tumor regrowth occur when dosing of GCV is terminated? Future studies using MRI/S may help to resolve some of these and other important issues. Once the therapeutic approach is optimized, localized *in vivo* MRS can then be correlated with cell kill to define the specific metabolite changes and expected time course for predicting therapeutic outcome in the clinical setting. The use of MRI/S in future gene therapy experimental protocols should greatly facilitate our understanding of how to optimize each new antitumor therapy.

The use of ^{19}F and ^{13}C MRS to noninvasively follow the metabolism of MRS-observable labeled precursors and offers an excellent opportunity to expand our understanding of the relatively obscure metabolic features which comprise the biochemistry of brain tumors. The study using (1-^{13}C)glucose to follow the degradation of glucose by the intracerebral C6 glioma in the rat demonstrates the unique information which can be gained by this approach (40). In this study, the label was transferred to a glycolytic product (lactate), tricarboxylic acid cycle intermediates (Glu/Gln) and surprisingly, glycogen. This study revealed alternative pathways for glucose metabolism which are not utilized appreciably under normal conditions by the brain (40). The utility of such metabolic abnormalities for aiding in the diagnosis of cell type, grade or treatment effectiveness have not yet been evaluated. These types of phenotypically expressed genetic abnormalities, which result in abnormal lactate or glycogen production. may be valuable for discerning the specific underlying changes which are characteristic of cell type or grade of brain tumors.

As discussed above, key merits of NMR imaging and spectroscopy in application to neuro-oncology have rationale based on the ability to non-invasively monitor gross morphology/volume and metabolism of tumors, with notable potential to serially monitor response to therapies. In addition, insight into tissue structure at the cellular level is available by quantitation of properties affected by the tissue water microscopic environment and

dynamics. MR] contrast itself has such a dependence embodied in NMR relaxation times T_1 and T_2. However, physical processes that determine T_1 and T_2 involve complex interactions of chemical, physical (i.e. molecular translation and rotation), and magnetic environments experienced by water. Rationale behind exploration of tissue water diffusion properties is based on the desire for a more direct measure of tissue/tumor cellularity and integrity of cellular membranes that impede water translational mobility. Water diffusion measurements have already been shown to be sensitive to tissue cellular structural anisotropy that is manifest as diffusion anisotropy (41, 48, 50). In addition, diffusion has been shown to be extremely valuable in model systems to study stroke (50). It is hoped that quantitative ADC measurements may also be a valuable probe in the study of CNS tumors and, more importantly, to guide more effective treatment protocols.

Conclusion and future prospects

MRI and MRS are important and complementary techniques for studying many aspects of brain tumors and can provide information not easily obtained by other methods. These techniques bridge the gap between cultured tumor cells, animal models and human studies and may be invaluable for endeavors involving the search for a cure for this disease and for aiding in the diagnosis and therapeutic management of patients. The results obtained thus far from MR studies of experimental brain tumors in rodents has already provided novel and fascinating insights into the biology, biochemistry, and effects of treatment on these model systems.

Gene transfer techniques are increasingly being developed and explored for the treatment of malignant primary tumors of the brain such as glioblastoma. Because the efficiency of the gene transfer procedure can vary for many reasons (including type of vector used, infection technique, stability of the particular gene and expressed protein, viral titer of injected solution, etc.), it would be especially valuable to have a method for non-invasive assessment of gene transfer effectiveness. The capability of *in vivo* MRS for monitoring cellular metabolites in intact biological tissues is especially attractive for such purposes. A specific example could be the use of localized MRS for the detection of the conversion of ^{13}C-labeled substrates into ^{13}C-labeled products by an enzyme expressed by gene transfer into a solid tumor.

This approach would offer an exciting and powerful method for regional assessment of the effectiveness of gene transfer into tumors and could merge the two seemingly disparate worlds of molecular biology and Radiology. Perhaps the advent of Molecular Radiology is indeed near.

Acknowledgments

We would like to thank Prof. Harry S. Greenberg for helfull comments.

This research was supported in part by grant BE-149 from the American Cancer Society and National Institutes of Health Grants R29 CA59009 and P20 NS31114. Oded Ben-Yoseph is a Fellowship recipient of the American Brain Tumor Association.

References

1. Walker MD, Green SB, Byar DP, Alexander E Jr, Batzdorf U, Brooks WH, Hunt WE, MacCarty CS, Mahaley MS Jr, Mealey J Jr, Owens G, Ransohoff J, Robertson JT, Shapiro WR, Smith KR Jr, Wilson CB, Strike TA. Randomized comparisons of radiotherapy and nitrosoureas for the treatment of malignant glioma after surgery. N Engl J Med. 1986; 303:1323–1329. [PubMed: 7001230]
2. Grossman SA, Burch PA. Quantitation of tumor response to antineoplastic therapy. Semin Oncol. 1988; 15:441–454. [PubMed: 3051401]
3. Levin VA, Crafts DC, Norman DM, Hoffer PB, Spire JP, Wilson CB. Criteria for evaluating patients undergoing chemotherapy for malignant brain tumors. J Neurosurg. 1977; 47:329–335. [PubMed: 894339]
4. Wilson CB, Crafts D. Criteria of response and definition of recurrence. Natl Cancer Inst Monogr. 1977; 46:197–203. [PubMed: 349397]
5. Grossman, SA. Chemotherapy of brain tumors. In: Salcman, M., editor. Concepts in neurosurgery. Vol. 4. Baltimore: Williams and Wilkins; 1991. p. 321-340.Neurobiology of brain tumors
6. Peterson DL, Sheridan PJ, Brown WE Jr. Animal models for brain tumors: historical perspectives and future directions. J Neurosurg. 1994; 80:865–876. [PubMed: 8169627]
7. Barker M, Hoshino T, Gurcay O, Wilson CB, Nielsen SL, Downie R, Eliason J. Development of an animal brain tumor model and its response to therapy with 1,3-bis(2-chloroethyl)-1-nitrosourea. Cancer Res. 1973; 33:976–986. [PubMed: 4703128]
8. Rosenbium ML, Wheeler KT, Wilson CB, Barker M, Knebel KD. *In vitro* evaluation of *in vivo* brain tumor chemotherapy with 1,3-Bis(2-chloroethyl)-1-nitrosourea. Cancer Res. 1975; 35:1387–1391. [PubMed: 1131813]
9. Rosenblum ML, Knebel KD, Vasquez DA, Wilson CB. *In vivo* clonogenic tumor cell kinetics following 1,3-bis(2-chloroethyl)-1-nitrosourea brain tumor therapy. Cancer Res. 1976; 36:3718–3725. [PubMed: 953998]
10. Rosenblum ML, Knebel KD, Vasquez DA, Wilson CB. Brain-tumor therapy. Quantitative analysis using a model system. J Neurosurg. 1977; 46:145–154. [PubMed: 833632]
11. Rosenblum ML, Deen DF, Hoshino T, Dougherty DA, Williams ME, Wilson CB. Comparison of clonogenic cell assays after *in vivo* and *in vitro* treatment of 9L gliosarcoma. Br J Cancer. 1980; 41(Suppl IV):307–308.
12. Wheeler KT, Wallen CA. Is cell survival a determininant of the *in situ* response of 9L tumours? Br J Cancer. 1980; 41(Suppl IV):299–303.
13. Rosenblum ML, Dougherty DA, Brown JM, Barker M, Deen DF, Hoshino T. Improved methods for disaggregating single cells from solid tumors. Cell Tissue Kinetics. 1980; 13:667.
14. Weizsaecker M, Deen DF, Rosenblum ML, Hoshino T, Gutin PH, Barker M. The 9L rat brain tumor: Description and application of an animal model. J Neurol. 1981; 224:183–192. [PubMed: 6162014]
15. Nomura K, Hoshino T, Pentecost SM. Post-treatment kinetics of BCNU in a 9L rat brain tumor model. Neurol Med Chir (Tokyo). 1981; 21:19–25. [PubMed: 6168947]
16. Wheeler KT, Kaufman K. Efficacy of continuous treatment with radiation in a rat brain-tumor model. J Neurosurg. 1981; 55:52–54. [PubMed: 7241215]
17. Vats TS, Kimler BF, Henderson SD, Morantz RA. Combination chemotherapy for the 9L rat brain tumor model system. Cancer Treat Rep. 1982; 66(3):575–579. [PubMed: 6174232]
18. Hill, RP. Experimental radiotherapy. In: Tannock, IF.; Hill, RP., editors. The basic science of oncology. New York: McGraw-Hill, Inc.; 1992. p. 276-301.
19. Ross BD, Merkle H, Henclrich K, Staewen RS, Garwood M. Spatially localized ^{1}H spectroscopy of a rat intracerebral glioma. Magn Reson Med. 1992; 23:96–108. [PubMed: 1734186]
20. Ordidge RJ, Connelly A, Lohman JAB. Image-selected *in vivo* spectroscopy (ISIS). A new technique for spatially selective NMR spectroscopy. J Magn Reson. 1986; 66:283–294.
21. Brown TR, Kincaid BM, Ugurbil K. NMR chemical shift imaging in three dimensions. Proc Natl Acad Sci USA. 1982; 79:3523–3526. [PubMed: 6954498]

22. Garwood, M.; Ross, BD.; Mitchell, SL.; Hendrich, K.; Merkle, H. ^{1}H spectroscopy using solvent suppressive adiabatic pulses (SSAP); 1988; 7th Annual Meeting of Society of Magnetic Resonance in Medicine; San Francisco, California.
23. Garwood M, Ugurbil K, Rath AR, Bendali MR, Ross BD, Mitchell SL, Merkle H. Magnetic resonance imaging with adiabatic pulses using a single surface coil for RF transmission and signal detection. Magn Reson Med. 1989; 9:25–34. [PubMed: 2709994]
24. Bitonti AJ, Dumont JA, Bush TL, Cashman EA, Cross-Doersen DE, Wright PS, Matthews DP, McCarthy JR, Kaplan DA. Regression of human breast tumor xenografts in response to (*E*)-2′-Deoxy-2′-(fluoromethylene)cytidine, an inhibitor of ribonucleotide diphosphate reductase. Cancer Res. 1994; 54:1485–1490. [PubMed: 8137252]
25. Moolten FL. Tumor chemosensitivity conferred by inserted herpes thymidine kinase genes: Paradigm for a prospective cancer control strategy. Cancer Res. 1986; 46:5276–5281. [PubMed: 3019523]
26. Culver KW, Ram Z, Wallbridge S, Ishii H, Oldfield EH, Blaese RM. In vivo gene transfer with retroviral vector-producer cells for treatment of experimental brain tumors. Science. 1992; 256:1550–1552. [PubMed: 1317968]
27. Ram Z, Culver KW, Walbridge S, Blaese RM, Oldfield EH. *In situ* retroviral-mediated gene transfer for the treatment of brain tumors. J Neurosurg. 1993; 79:400–407. [PubMed: 8395592]
28. Ram Z, Walbridge S, Shawker T, Culver KW, Blaese RM, Oldfield EH. The Effect of thymidine kinase transduction and ganciclovir therapy on tumor vasculature and growth of 9L gliomas in rats. J Neurosurg. 1994; 81:256–260. [PubMed: 8027810]
29. Oldfield EH, Ram Z, Culver KW, Blaese RM, DeVroom HL, Anderson WF. Gene therapy for the treatment of brain tumors using intratumoral transduction with the thymidine kinase gene and intravenous ganciclovir. Hum Gene Ther. 1993; 4:39–69. [PubMed: 8384892]
30. Ben-Yoseph O, Ross BD. Oxidation Therapy: The use of a reactive oxygen species-generating enzyme system for tumour treatment. Br J Cancer. 1994 In press.
31. Schraufstatter IU, Hyslop PA, Hinshaw DB, Spragg RG, Sklar LA, Cochrane CG. Hydrogen peroxide-induced injury of cells and its prevention by inhibitors of poly(ADP-ribose) polymerase. Proc Natl Acad Sci USA. 1986; 83:4908–4912. [PubMed: 2941760]
32. Berger NA. Cancer chemotherapy: New strategies for success. J Clin Invest. 1986; 78:1131–1135. [PubMed: 3533996]
33. Ueda K, Hayaishi O. ADP-ribosylation. Annu Rev Biochem. 1985; 54:73–100. [PubMed: 3927821]
34. Bruchelt G, Schraufstatter IU, Niethammer D, Cochrane CG. Ascorbic acid enhances the effects of 6-hydroxydopamine and H_2O_2 on iron-dependent DNA strand breaks and related processes in the neuroblastoma cell line SK-N-SH. Cancer Res. 1991; 51:6066–6072. [PubMed: 1933870]
35. Brodie AE, Reed DJ. Reversible oxidation of glyceraldehyde 3-phosphate dehydrogenase thiols in human lung carcinoma cells by hydrogen peroxide. Biochem Biophys Res Commun. 1987; 148:120–125. [PubMed: 3675570]
36. Paggi MG, Zupi G, Fanciulli M, Carlo CD, Giorno S, Laudonio N, Silvestrini B, Caputo A, Floridi A. Effect of lonidamine on the utilization of ^{14}C-labeled glucose by human astrocytoma cells. Exp Mol Pathol. 1987; 47:154–165. [PubMed: 2820786]
37. Ward-Hartley KA, Jain RK. Effect of glucose and galactose on microcirculatory flow in normal and neoplastic tissues in rabbits. Cancer Res. 1987; 48:371–377. [PubMed: 3791228]
38. Ross BD, Mitchell SL, Merkle H, Garwood M. In vivo ^{31}P and ^{2}H NMR studies of rat brain tumor pH and blood flow during acute hyperglycemia: Differentail effects between subcutaneous and intracerebral locations. Magn Reson Med. 1989; 12:219–234. [PubMed: 2559287]
39. Kim SG, Ackerman JH. Quantitative determination of tumor blood flow and perfusion *via* deuterium nuclear magnetic resonance spectroscopy in mice. Cancer Res. 1988; 48:3449–3453. [PubMed: 2836055]
40. Ross BD, Higgins RJ, Boggan JE, Willis JA, Knittel B, Unger SW. Carbohydrate metabolism of the rat C6 glioma. An *in vivo* ^{13}C and *in vitro* ^{1}H magnetic resonance spectroscopy study. NMR in Biomed. 1988; 1:20–26.

41. Chenevert TL, Brunberg JA, Pipe JG. Anisotropic diffusion in human white matter: Demonstration with MR techniques in vivo. Radiology. 1990; 177:401–405. [PubMed: 2217776]

42. Kim, B.; Ross, BD.; Chenevert, TL.; Sunkara, PS.; McCarthy, JR. Validation and application of MRI for assessing therapeutic efficacy of experimental intracranial gliomas; 1993; 12th Annual Meeting of Society of Magnetic Resonance in Medicine; New York, New York.

43. Kim B, Chenevert TL, Ross BD. Assessment of growth rate and therapeutic efficacy of the rat 9L brain tumor model using magnetic resonance imaging. Clinical Cancer Res. 1994 submitted.

44. Kim, B.; Chenevert, TL.; Sunkara, PS.; McCarthy, JR.; Ross, BD. ^{1}H MRS and MRI studies of the antitumor activity of (E)-2′-deoxycytidine(FMdc, MDL 101,731) on experimental intracranial gliomas; 1993; 12th Annual Meeting of Society of Magnetic Resonance in Medicine; New York, New York.

45. Kim, B.; Chenevert, TL.; Ross, BD. Quantitating treatment of rat intracerebral tumors using MRI volumetric measurements: A standard for correlative spectroscopic studies; 1994; 2nd Annual Meeting of Society of Magnetic Resonance; San Francisco, CA.

46. Kim, B.; Davidson, BL.; Shewach, D.; Hurlbert, C.; Ross, BD. Assessment of efficacy of ganciclovir toxicity following adenoviral mediated gene transfer of the HSV-TK gene to experimental intracranial gliomas using ^{1}H MRS and MRI; 1994; 2nd Annual Meeting of Society of Magnetic Resonance; San Francisco, CA.

47. Ben-Yoseph, O.; Gillies, RJ.; Lyons, JC.; Song, CW.; Ross, BD. ^{31}P NMR studies of lonidamine (LND) on gliomas suggests mechanism of action involves inhibition of mitochondrial-bound hexokinase; 1993; 12th Annual Meeting of Society of Magnetic Resonance in Medicine; New York, New York.

48. Chenevert, TL.; Ross, BD.; Pipe, JG.; Simerville, SJ. Quantitative diffusion anisotropy in rat gliomas; 1991; 10th Annual Meeting of Society of Magnetic Resonance in Medicine; San Francisco.

49. Ward KA, Jain RK. Response of tumours to hyperglycaemia: Characterization, significance and role in hyperthermia. Int J Hyperthermia. 1988; 4:223–250. [PubMed: 3290346]

50. Le Bihan D. Molecular diffusion nuclear magnetic resoance imaging. Magn Reson Quart. 1991; 7:1–30.

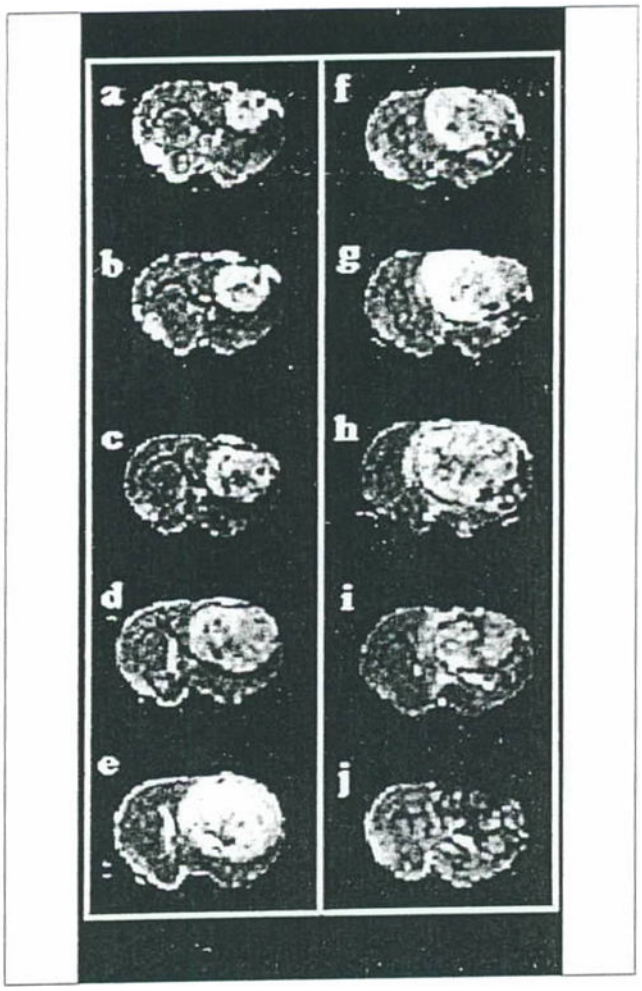

Figure 1.

Coronal brain T_2-weighted images of two rats at various times post-implantation of 9L tumor cells. Images A–E are from an untreated 9L tumor rat at days 10, 12, 14, 16 and 18 days post-implantation, respectively. Images F–J are from a second rat 9L tumor at days 14, 17, 20, 24 and 28 days post-implantation, respectively. Two hr prior to acquiring the 14 day image (Image F) the rat was treated with a single dose of BCVU (13.3 mg/kg, i.p.). The tumor continued to expand until day 20 post-implantation and a heterogeneous reduction in tumor image intensity was noted at later times following treatment (images I and J).

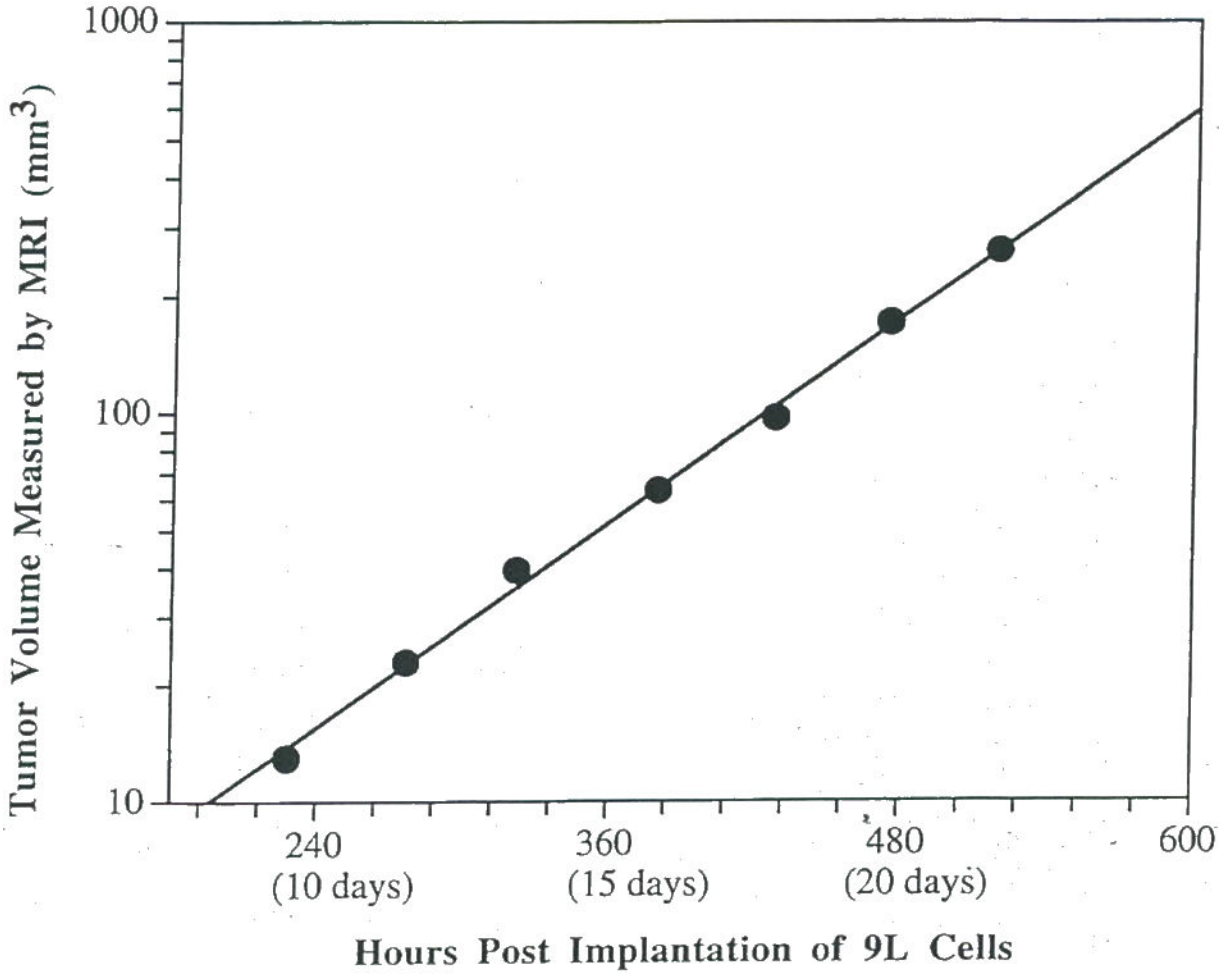

Figure 2.

A plot of the MRI-determined untreated intracerebral 9L rumor volume versus time post-implantation. The volume measurements are shown along with a line corresponding to the least squares fit to the experimentais data. This plot reveals the exponential growth of the intracerebral 9L tumor which is characteristic of all 9L rumors examined to date.

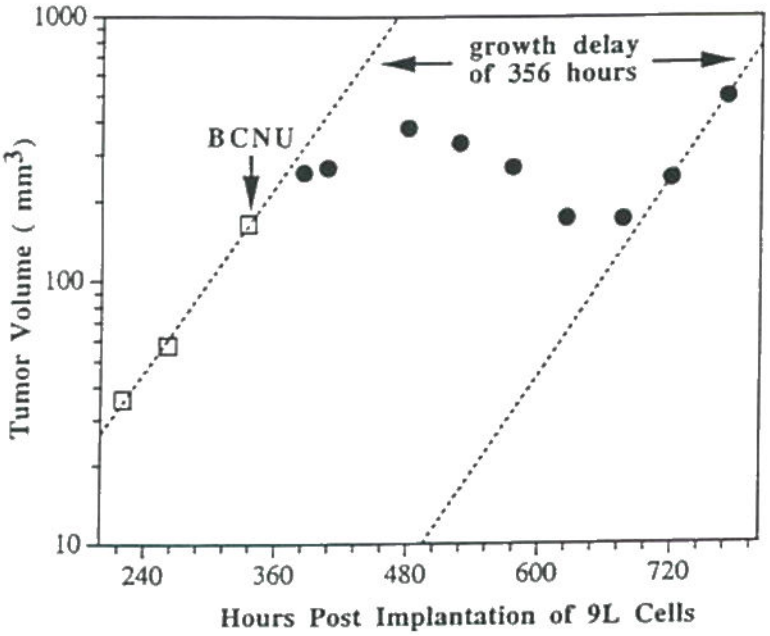

Figure 3.

A plot of MRI-determined intracerebral (umor volume versus time post-implantation for an intracranial 9L tumor treated with an LD_{10} dose (13.3 mg/kg, i.p.) of BCNU at 350 hr. post-implantation. The initial three tumor volume measurements were used to determine the pre-treatment T_d which was determined to be 49 hr. Following BCNU adminbtration (denoted by downward pointing arrow), the tumor volume continued to increase but at a greatly reduced rate which was followed by a slight tumor regression. Regrowth of the tumor occurred at approximately 706 hr. post-implantation at a calculated rate of 51 hr. A growth delay of 356 hr. (approx. 15 days) was observed for this tumor.

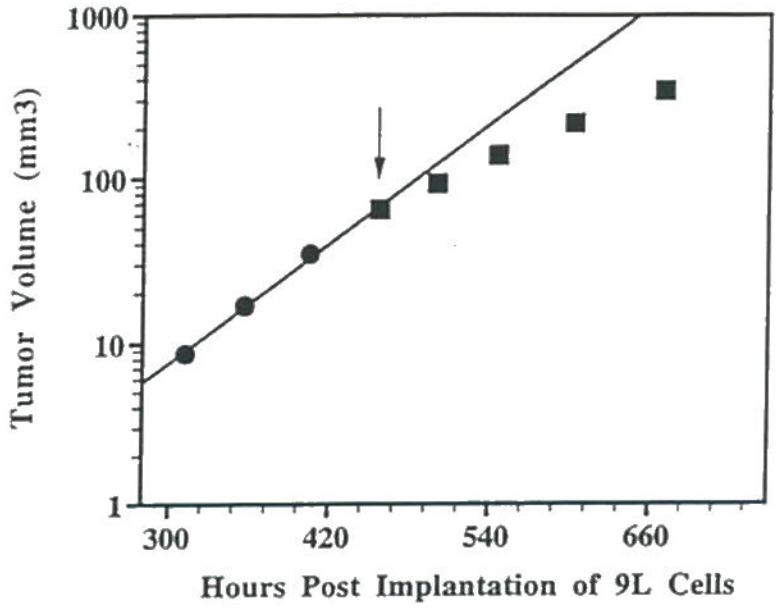

Figure 4.

A plot of MRI-determined intracerebral tumor volume versus time post-implantation for an intracranial 9L tumor treated daily with FMdc (15 mg/kg. i.p.) beginning at 460 hr. post-implantation (indicated by the downward pointing arrow). The initial T_d was determined to be 50 hr. After 4 and 8 days of treatment with FMdc. the T_d decreased to 81 and 95 hr., respectively. This data reveals a significant therapeutic effect of FMdc on intracranial 9L rumor growth.

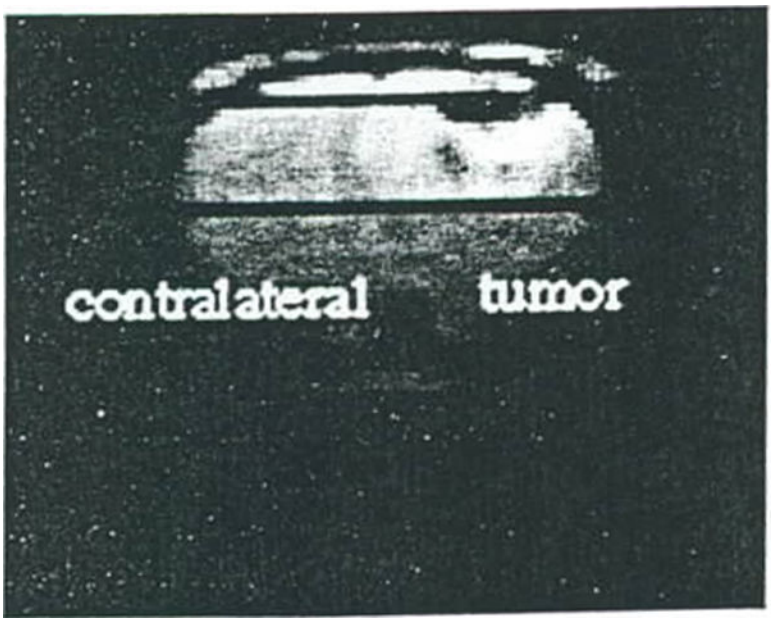

Figure 5.
Surface coil coronal T_2-weighted MR image of a rat brain with a 9L tumor. Position of the ISIS column used for obtaining the localized ^1H spectra is shown by the dark lines.

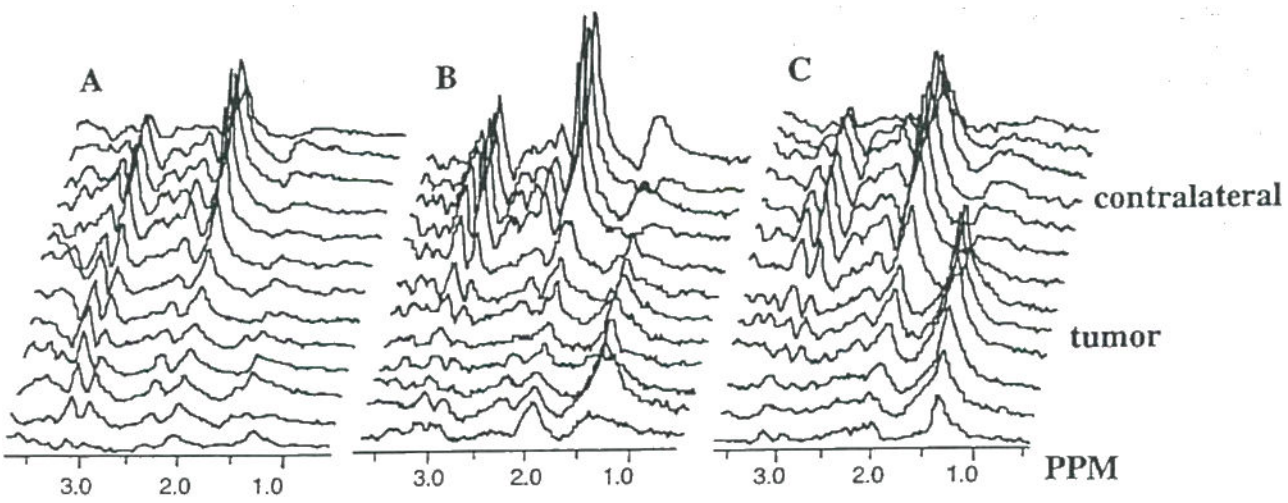

Figure 6.

Spatially localized ^{1}H spectra obtained from a rat brain with an (A) untreated 9L tumor and a 9L tumor treated for (II) 6 days and (C) 9 days with FMdc (15 mg/kg. i.p.). Spectra reveal a progressive increase in the lipid/lactate resonance intensity (1.3 ppm) and a decrease in the choline (3.2 ppm) and creatine (3.0 ppm) resonances.

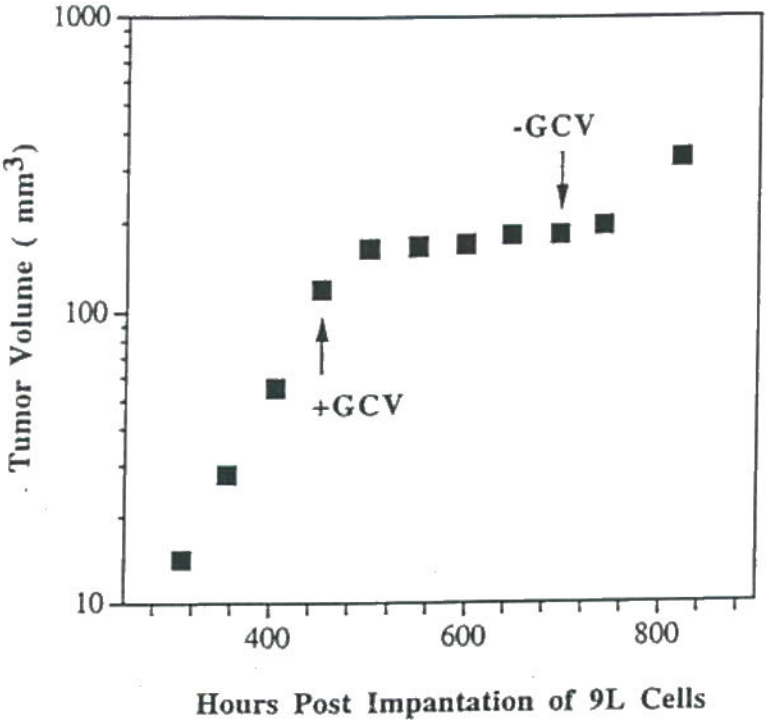

Figure 7.

A plot of MRI-determined intracerebral rumor volume versus time post-implantation for an intracranial 9L tumor treated with Ad.RSVtk/GCV beginning at the position of the upward pointing arrow. GCV administration (15 mg/kg, i.p. 2 × daily) was discontinued at the time indicated by the downward pointing arrow. This data reveals Ad.RSVtk/GCV produced a significant therapeutic effect on intracranial 9L tumor growth. Tumor regrowth occurred shortly following termination of GCV administration.

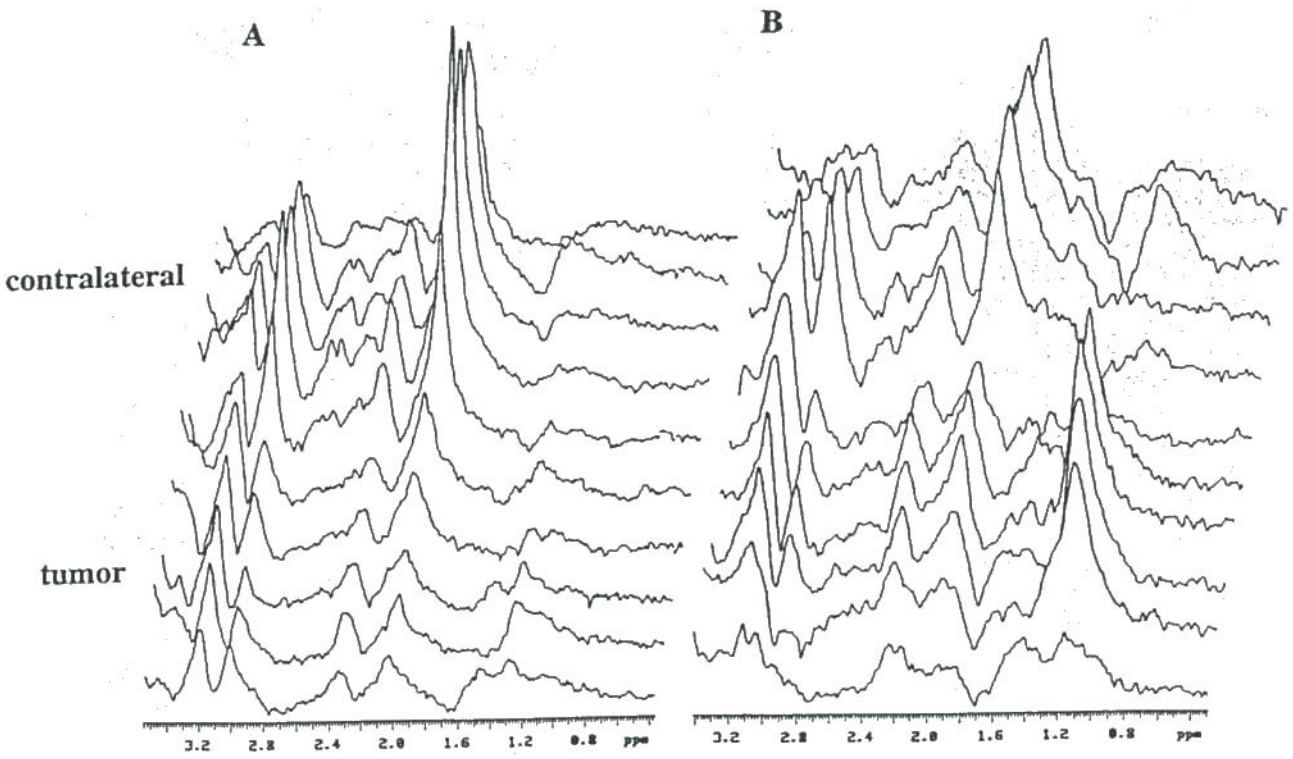

Figure 8.

Spatially localized ^{1}H spectra obtained from a rat brain with an (A) untreated 9L tumor and (B) a 9L tumor treated for 7 days with GCV (15 mg/kg. i.p. 2 × daily) following intratumoral injection with Ad.RSVtk. Spectra from treated 9L tumors consistently revealed an increase in the lipid/lactate resonance intensity (1.3 ppm).

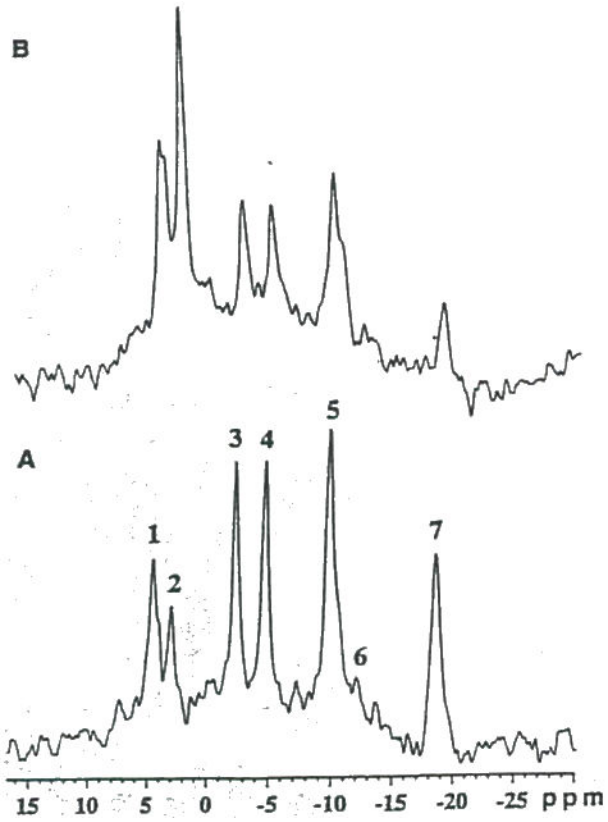

Figure 9.

In vivo ^{31}P MR spectra of a subcutaneous 9L tumor obtained (A) before, and 6 hr. following intratumoral administration of (B) 50 units PEG-GO. Resonance assignments are as follows: 1, phosphomo-nocsters (PME); 2, inorganic phosphate (P_i); 3, phosphocreatine (PCr); 4, γ-ATP and β-ADP; 5. α-ATP. α-ADP and NAD^+/NADH; 6, diphosphodicster; and 7, β-ATP.

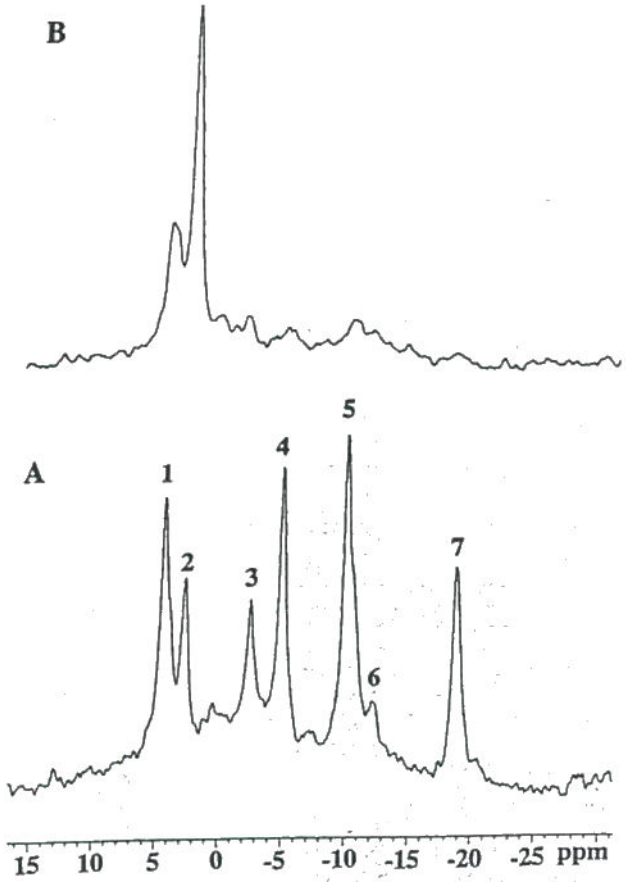

Figure 10.

In vivo ^{31}P MR spectra of a subcutaneous 9L tumor obtained (A) before, and 6 hr. following intratumoral administration of (B) 2 × 200 units PEG-GO. Resonance assignments are identical to figure 9.

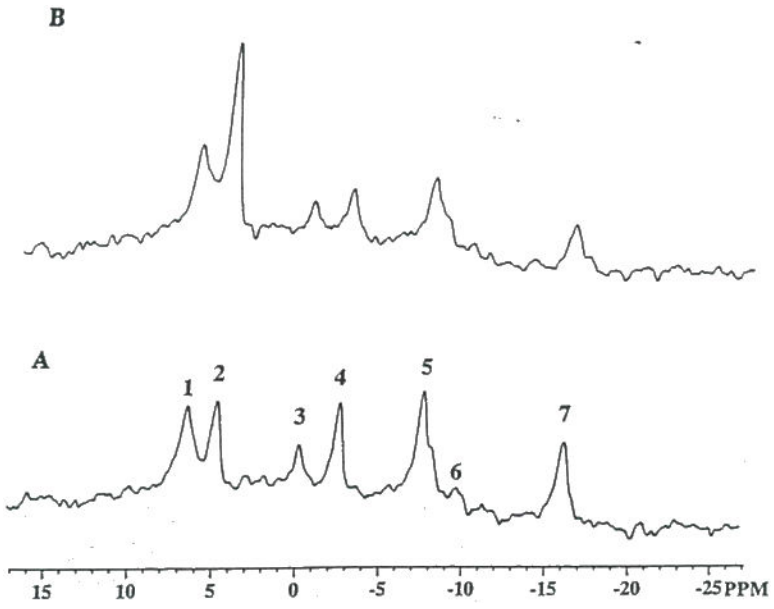

Figure 11.

In vivo ^{31}P MR spectra of a subcutaneous 9L tumor (A) pre- and (B) 3 h post-administration of LND (100 mg/kg, i.p.). Phosphorus-containing metabolites are identified as shown in figure 9 Note the dramatic decline in ATP levels and the corresponding increase in the hydrolysis product, P_i indicating impaired energy metabolism.

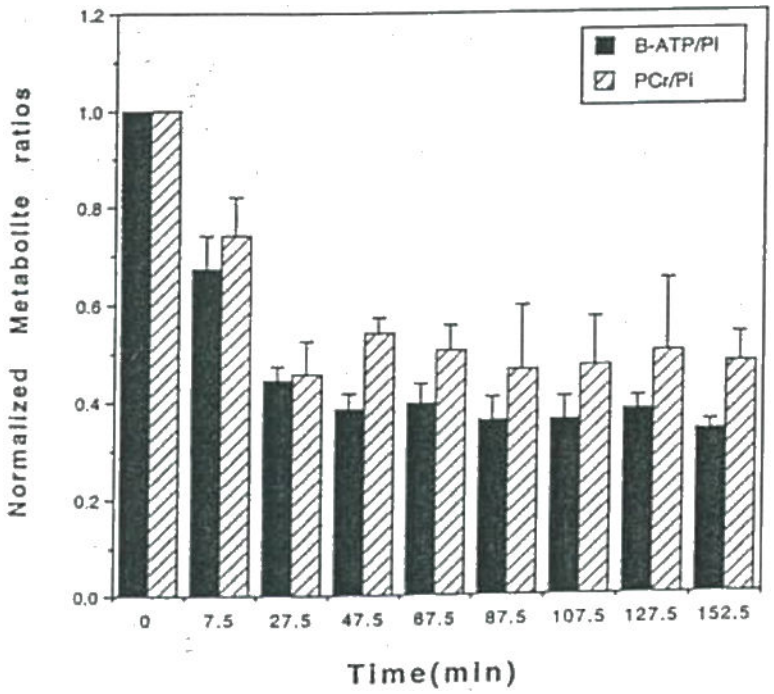

Figure 12.

Time course of the average subcutaneous 9L tumor (n=3) b. ATP/P_i and PCr/P_i ratios following administration of LND at time=0. Values are plotted at the average time during which the spectra were accumulated. Error bars represent ±SEM.

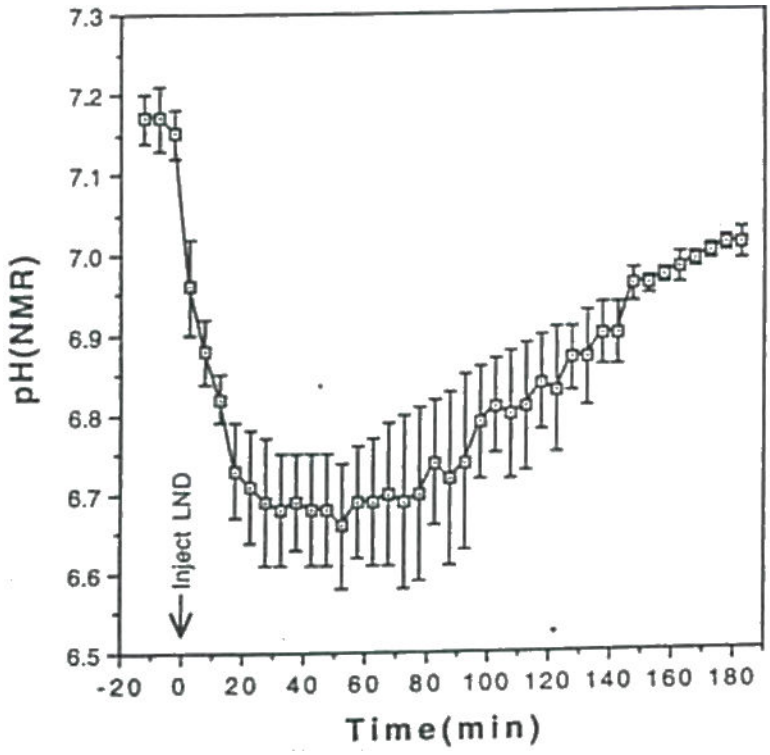

Figure 13.

Time course of the average subcutaneous 9L tumor (n=3) pH following injection of LND at time=0. The average pH values are plotted with ±SEM.

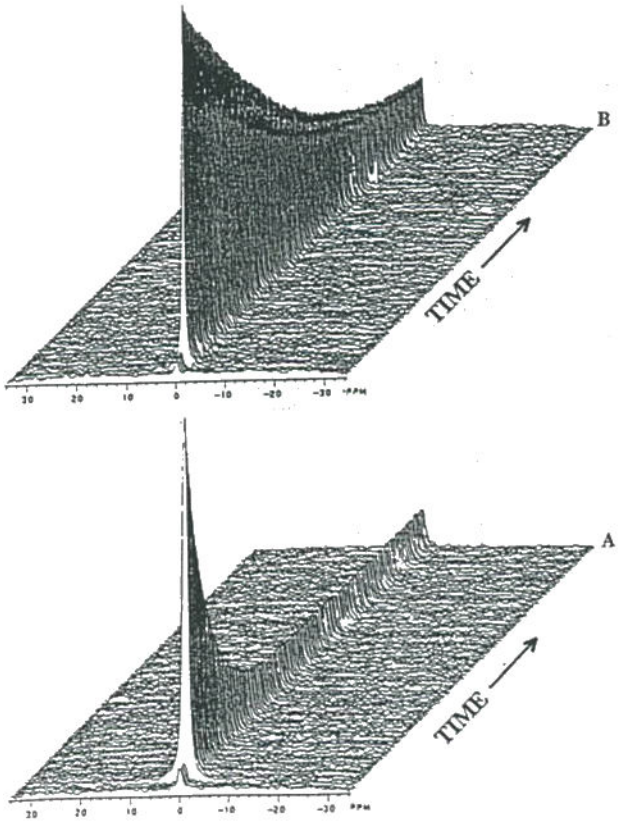

Figure 14.

In vivo ^{2}H MRS of $^{2}H_2O$ washout of a subcutaneous C6 glioma following a two-site intratumoral injection. Spectra are from the same tumor (A) before and (B) 1 hr following initiation of acute hyperglycemia via administration of a bolus of 6g/kg (i.p.) of a 50% glucose solution. In each case three pre-injection ^{2}H spectra were acquired before injection of $^{2}H_2O$ saline. Each spectrum represents an average of 30 sec. acquisition time. ^{2}H spectra were adapted from reference (38).

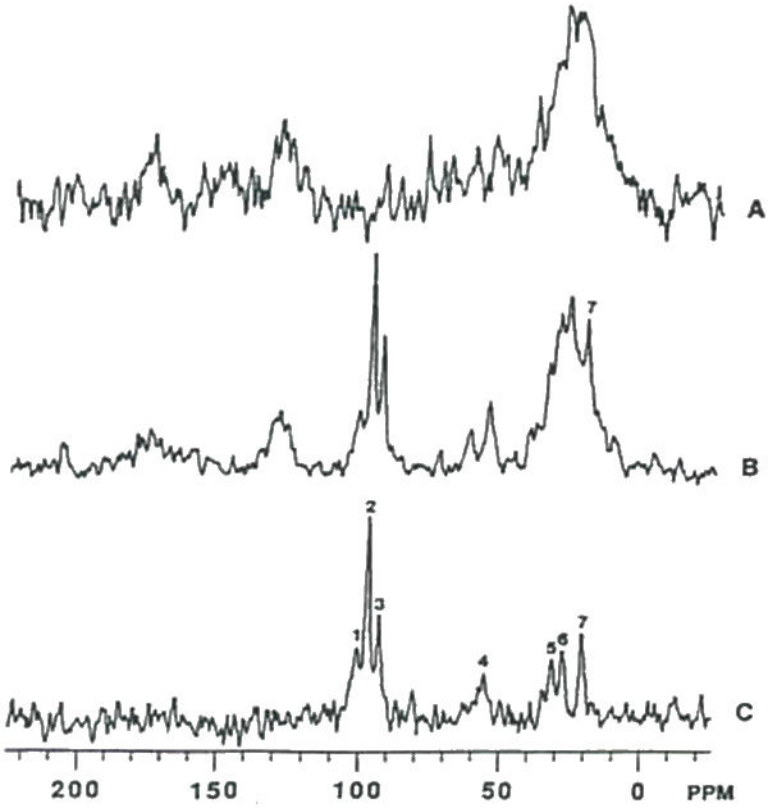

Figure 15.

In vivo ^{13}C MR spectra of an intracerebral C6 glioma. (A) Natural abundance spectra from an acquisition time of 46.8 minutes. (B) Spectrum from the same C6 glioma which was acquired over a 93.6 minute time interval during a constant infusion with (1-^{13}C)glucose. (C) Difference spectrum obtained following subtraction 2 times the spectrum (A) from spectrum (B). Resonance assignments are as follows: 1. C-1 carbon of glycogen; 2. β-glucose; 3. α-glucosc; 4. C-2 carbon of Glu/Gln; 5. C-4 carbon of Glu/Gln; 6. C-3 carbon of Glu/Gln; and 7. C-3 carbon of lactate. ^{13}C spectra were adapted from reference (40).

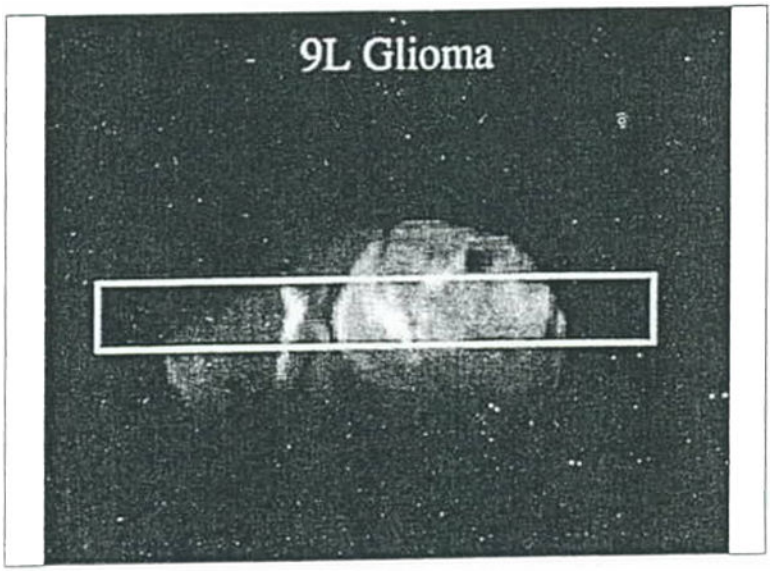

Figure 16.

Water diffusion study on rat brain with a 9L tumor. Surface coil coronal T_2-weighted MR image of a rat brain with the column used for obtaining the diffusion data scribed on the image.

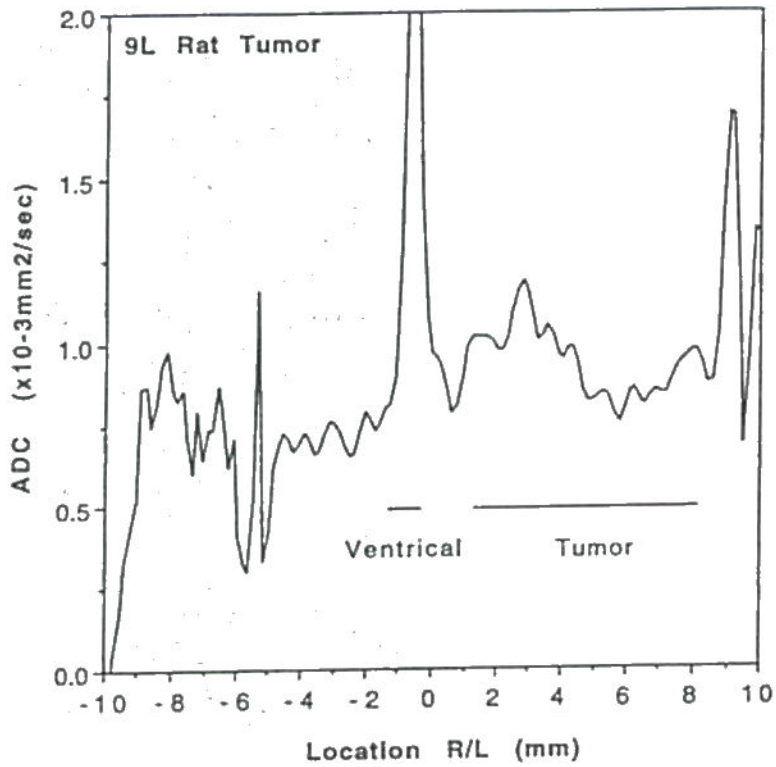

Figure 17.

Plot of water ADC_{mean} (mean of ADCx, ADCy, and ADCz) as a function of position along the column shown in Figure 16. Note, the ADC_{mean} in the tumor is only moderately elevated relative to contralateral brain tissue.

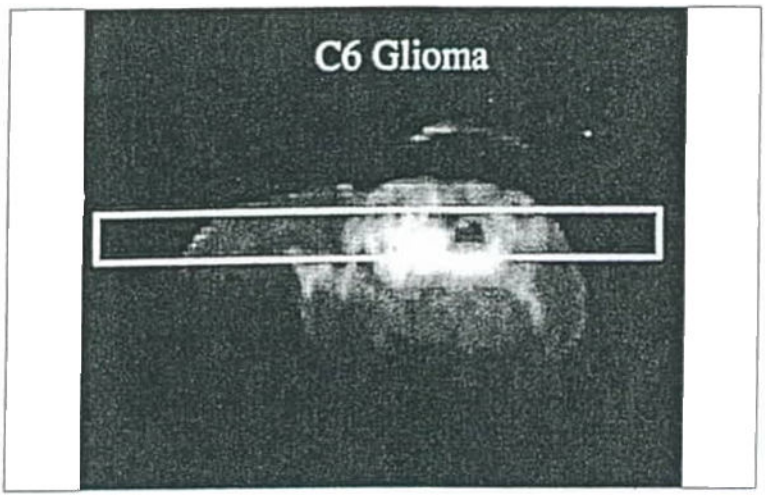

Figure 18.

Water diffusion study on rat brain with a C6 tumor. Surface coil coronal T_2-weighled MR image of a rat brain with the column used for obtaining the diffusion data scribed on the image.

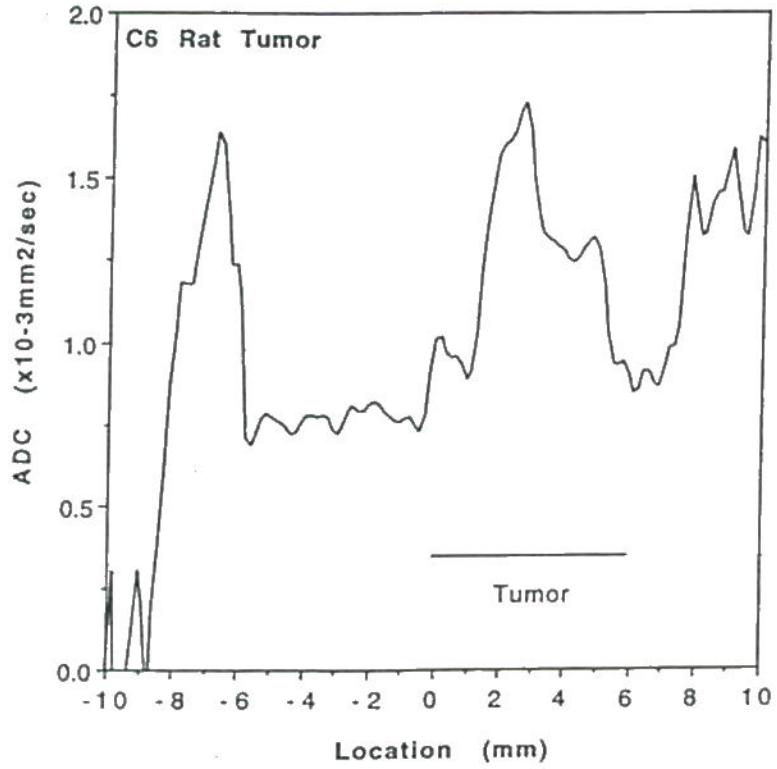

Figure 19.

Plot of water ADC_{mean} as a function of position along the column shown in Figure 18. Note, the ADC_{mean} in the tumor is significantly elevated relative to contralateral brain and 9L tumor (cf Figure 17) indicating greater free water space and mobility associated with necrosis.

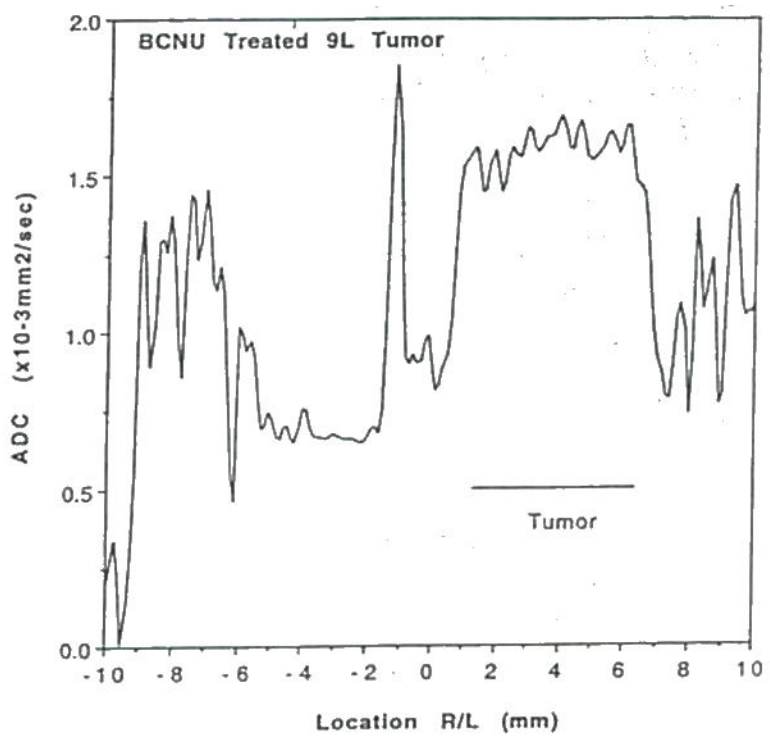

Figure 20.

Water diffusion study on a BCNU treated intracerebral 9L tumor at 10 days post BCNU administration and 25 days post tumor implant. Plot of water ADCmean as a function of position through the tumor and contralateral brain. Note, the ADC in the treated tumor is significantly elevated relative to contralateral brain tissue and non-treated 91. tumor values (cf Figure 17).